A Numerical Investigation of wake and mixing layer interactions of Flow past a Square Cylinder

Aditya. Mushyam[1] and Josep M Bergada
Fluid Mechanics Department
Technical University of Catalunya
Terrassa, Barcelona, Spain-08222
[1]Corresponding author

[1]Corresponding Author:
Aditya Mushyam
Doctorate Researcher
Department of Fluid Mechanics
Technical University of Catalunya
Terrassa, Barcelona-08222
Email:mushyam.aditya@gmail.com
Phone: +34632771104

Josep M Bergada
Associate Professor
Department of Fluid Mechanics
Technical University of Catalunya
Terrassa, Barcelona-08222
Email: bergada@mf.upc.edu
Phone: +34937398771

A Numerical Investigation of wake and mixing layer interactions of Flow past a Square Cylinder

Aditya Mushyam[1] and Josep M Bergada
Fluid Mechanics Department
Technical University of Catalunya
Terrassa, Barcelona, Spain-08222
[1]Corresponding author

Abstract:
The aim of the present study is to simulate and analyze the interaction of two dimensional flow past a square cylinder in a laminar regime with an upstream mixing layer developed by an axis symmetrical horizontal splitter plate. The mixing layer is generated upstream of the square cylinder by mixing two uniform streams of fluid with different velocities above and below the splitter plate. A range of upstream domain lengths, distances between the splitter plate and the square cylinder, and upstream velocity ratios between the two streams of fluid are analyzed. Unconfined flow over a square cylinder placed in uniform upstream flow is initially analyzed as it plays a crucial role in understanding the properties of the wake. The results are compared with the existing literature to validate the code developed and they are found to be in very good agreement. It is observed from the present study that at smaller velocity ratios, the vortices shed into the wake consist of both clockwise and anticlockwise moment vortices. As velocity ratio is increased only clockwise moment vortices are shed downstream and anticlockwise vortices are shed as Kelvin-Helmholtz instabilities. In all simulations undertaken the same phenomena is observed independent of the upstream Reynolds number, indicating that velocity ratio is a primary parameter influencing the flow. Different instability modes were observed and they were highly dependent on the upstream velocity ratio.

Keywords: Square cylinder, Mixing layer, Splitter plate, Wake-Mixing Layer Interaction, Laminar Flow

Nomenclature:

a	Side of the square cylinder	
A	Dimensional side of the square cylinder	[m]
C_D	Drag coefficient	
C_L	Lift coefficient	
f	Dimensional frequency	[Hz]
F_D	Dimensional drag force	[N]
F_f	Flux through face f of the control volume	
F_L	Dimensional lift force	[N]
H	Height of the domain	
L	Length of the domain	
$\hat{n}$	Outward normal of the surface S	
p	Non dimensional Pressure	
r	Ratio of Reynolds number above and below the splitter plate	
Re	Reynolds number	

S	Surface onto the control volume	
St	Strouhal number	
spl	Length of the flat plate	
t	Non-dimensional Time	
ul	Upstream Length of the physical domain	
dl	Downstream length of the physical domain	
dt	Non dimensional time step	
u	Non-dimensional Velocity in X direction below the splitter plate	
U	Free stream velocity in X direction at the inlet below the splitter plate [m/sec]	
v	Non-dimensional Velocity in Y direction	
$\forall$	Control Volume	
x	Non-Dimensional Eulerian coordinates in horizontal direction	
y	Non-Dimensional Eulerian coordinates in vertical direction	
ρ	Fluid density.	[Kg/m^3]
μ	Fluid viscosity	[Kg/(m s)]

1. Introduction.

Studies on the problems of wake development and vortex shedding behind a rectangular/square cylinder in free-stream flows was investigated both numerically and experimentally among others by, Franke (1991), Franke et al. (1990), Kelkar and Patankar (1992), Davis and Moore (1982), Davis et al. (1984), Okajima (1982, 1990), Okajima et al (1992), Mukhopadhyay et al. (1992), Suzuki et al. (1993) and Sohankar et al (1998, 1999).

Based on experimental investigations, Okajima (1982), working with rectangular cylinders, found periodic vortex motion at Re=70. A smaller critical Reynolds for periodic vortex motion, Re=54, was determined by Kelkar and Patankar (1992) based on the flow stability analysis, they studied unconfined flow past a square cylinder. With a further increase of the Reynolds number, the flow undergoes a further bifurcation at around Re=150–200, Sohankar et al (1999), and becomes three-dimensional but remains time periodic. In reality, the onset of this phenomenon is not clearly defined in the literature, Okajima (1982) and Franke (1991), defined a range of Re=100 to 150 for the 3D bifurcation to appear. Luo et al (2003), (2007), experimentally studied the transition phenomena generated by uniform flow onto a square cylinder. They found two instability modes similar to the ones found by Williamson (1996) in circular cylinders.

It was shown by previous investigations on circular cylinders, e.g., Jordan and Fromm (1972), Kiya et al. (1980), Kwon et al. (1992), Mukhopadhyay et al. (1999), Xu and Dalton (2001), Sumner and Akosile (2003), that the flow approaching with linear shear greatly alters the vortex dynamics in the wake, when compared to the uniform flow case. They attributed this phenomenon to the constant vorticity embedded in the free-stream. For square-sectional cylindrical bodies, shear flow effects were reported by, e.g., Ayukawa et al. (1993), Hwang and Sue (1997), Saha et al. (2001), Bhattacharyya and Maiti (2004, 2006), Cheng et al. (2005, 2007) and Lankadasu and Vengadesan (2008). Saha et al. (2001) studied the same problem numerically for a wide range of Reynolds numbers. They showed that due to the influence of shear, Karman Vortex Street mainly consisted of clockwise vortices, whose decay was very slow when compared to that of uniform flow. Cheng et al.

(2005, 2007) reported that vortex shedding disappeared for large shear parameters. The mean lift and drag coefficients tended to decrease with increasing the shear parameter. They also observed that the vortex shedding frequency tended to decrease with the increase of the shear parameter, although they highlighted that this observation was opposite to the one obtained by Kiya et al. (1980) when studying shear flow past circular cylinders.

Lankadasu and Vengadesan (2008) also reported a decrease in the mean lift and drag coefficients with increasing shear, and for a given Reynolds number. The same phenomenon was observed for a given shear when the Reynolds number was increased. It was also found that the critical Reynolds number at which the flow becomes unsteady periodic, was reduced as shear increased. Bhattacharyya and Maiti (2004, 2006) studied laminar shear flow past a square cylinder placed near a wall, for Reynolds up to 1400. For a gap height of 0.25 times the square cylinder height, vortex shedding suppression and steadiness of the wake was observed up to a Reynolds 250. For a Reynolds number equal and above 500, only negative vortices behind the cylinder at closed proximity to the wall were found. They also investigated laminar flow over a square cylinder placed nearby a wall, Reynolds <1500, and found that the critical gap height for vortex shedding suppression was dependent on the Reynolds number.

There are typical situations, where the non-uniformity of the approaching flow is due to the effect of a body located in front of or behind the one to be studied. For example, when a small cylinder is placed in the separated shear layer of a large main cylinder to alter the vortex shedding phenomena behind the main cylinder, the small cylinder is inevitably subjected to the effect of shear induced from the large cylinder. The onset of periodic flow from the small cylinder induces oscillatory forces on the body, which may trigger flow-induced vibrations, and in turn alter the vortex shedding on the main cylinder.

Some of the most relevant recent numerical simulations of flow past a square cylinder with the incorporation of a control plate to alter the wake, which have close similarities to the present study, were carried out among others by Lesage and Gartshore (1987), Sakamoto et al (1991, 1997), Zhou et al (2005), Doolan (2009), Sukri et. al. (2011), (2012), Malekzadeh and Sohankar (2012) and Salinas et al (2014). Some of these studies are presented below.

Sukri et. al. (2011), carried out a 2D numerical study for flow over a square cylinder with and without a splitter plate at Reynolds number, Re=150. The splitter plate was stationary and attached to the square cylinder's trailing face. Strong hydrodynamic interactions in the near wake of the cylinder were induced by the splitter plate and the length of the plate was found to significantly affect the flow structure. In the study, flow behavior was categorized into three different modes based on the length of the splitter plate. The first mode occurred for splitter plate lengths in the range of $0 \leq L \leq D$, it was observed that the free shear layers were convected further downstream before rolling up and the Strouhal number decreased as the plate length was increased. When the splitter plate length L, was increased to 1.25D, a sharp increase in the Strouhal number was found, indicating the onset of a new mode. This second mode appeared, for intermediate lengths in the range of $1.25D \leq L \leq 4.75D$; a secondary vortex was reported to be seen around the trailing edge of the splitter plate and the shear layers began to roll up closer to the trailing edge. The Strouhal number in this mode first increased with the increase in length of the splitter plate until L=2D, before

decreasing with the increase in the length of the splitter plate until L=4.75D. When the length of the splitter plate was L ≥ 5D, a sudden decrease in the Strouhal number was found, indicating the onset of the third mode. In Sukri et. al (2012), a 2D numerical study of the square cylinder wake alteration using a detached downstream thin flat plate was carried out. A uniform upstream flow with constant Reynolds number Re=150, based on the side length of the cylinder D, was used. A critical gap distance of G_c=2.3D was reported, indicating the existence of two flow modes. Mode I was characterized by the completion of the vortex formation occurring downstream of the gap, but for mode II, formation was found to be occurring within the gap. The plate was found to have no effect on the formation of the Von-Karman vortex street for a gap G≥5.6D. With the aim to achieve total lift cancellation, the plate length was reduced and it was found that for a plate of length L=0.26D at G = 5.6D, located downstream of the square cylinder, a significant reduction in the lift fluctuation of the system was obtained, although a total lift cancellation was not observed. The reason behind non-occurrence of total lift cancellation was identified as the loss of fluctuating lift signal sinusoidal form, due to the plate undergoing stall.

Malekzadeh and Sohankar (2012), performed a 2D numerical investigation to reduce the fluid forces acting on a square cylinder in laminar flow regime by using passive flow control. The results of the heat transfer from the square cylinder in the presence of a control plate were also presented at a constant Reynolds number, Re=160 and Prandtl number, Pr=0.71. It was reported that the optimum plate-cylinder distance and control plate width, were respectively 3D and 0.5D. Three different flow modes were discovered at this Reynolds number, the vortex shedding from the control plate was completely suppressed in modes I and II, in mode III the Karman vortex street was generated behind the control plate and cylinder. Independently of the flow mode, the incorporation of the control plate significantly reduced the mean and fluctuating fluid forces on the cylinder.

In Salinas et al (2014), a LES 3D numerical analysis of a square cylinder with a vertical flat plate placed upstream was presented. Three different flow configurations were observed, in the first one, two quasi-stationary symmetric vortices were formed between the two bodies. The second configuration was characterized by asymmetric vortices appearing between the plate and the square cylinder. The appearance of fully developed turbulence in the wake behind the plate was defined as the third configuration.
Despite the fact that the present study has many similarities to the ones just presented, according to the authors knowledge this is the first time interaction between the wake of square cylinder and mixing layer has been numerically simulated and analyzed.

2. Problem Statement.

2.1 Physical and computational domains.

Figure 1 presents the physical domain with a square cylinder and a splitter plate placed upstream of the cylinder. The computational domain consists of a two-dimensional square cylinder of non-dimensional side length, a. The inlet boundary consists of two uniform fluid streams of different velocities above and below the splitter plate, as seen in figure 1. The ratio of velocities above and below the splitter plate is defined as velocity ratio, r. The computational domain length, L and height, H are taken as 32 times and 16 times the square cylinder length respectively, as seen in figure 1.

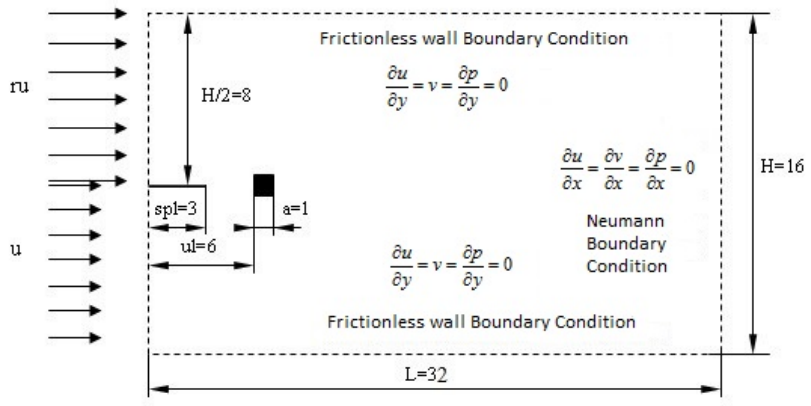

Figure 1: Physical Domain of the Inclined Step

According to Sohankar et al (1998), when using Neumann boundary conditions, a minimum downstream length of 20 times the square cylinder side length is required to isolate the effects of outlet boundary on the flow and wake properties. In the present study a downstream length of dl=25a units was considered for all cases simulated.

A frictionless wall boundary condition is applied to the top and bottom boundary of the physical domain as presented in figure 1. In Sohankar et al (1995), flow past a square cylinder was analyzed with frictionless wall boundary conditions with a blockage ratio of 7%, which converts to a physical domain height slightly higher than 14 units. It was observed that the boundary conditions above and below were not adversely affecting the flow behavior. Yoshida et al (1993), when studying unconfined flow past a square cylinder, used a height of 16 units for the physical domain and reported that boundary conditions had no effect on the flow. Therefore, for the present study, the physical domain height was taken as 16 units to make the flow independent of boundary conditions at the top and bottom of the physical domain. Three different upstream lengths ul, the distance between inlet and the square cylinder leading edge, were studied, namely ul=5a, 6a and 7a. For all three cases a constant splitter plate length, spl=3a, was considered in order to facilitate the development of laminar boundary layer. Splitter plate thickness was considered to be negligible.

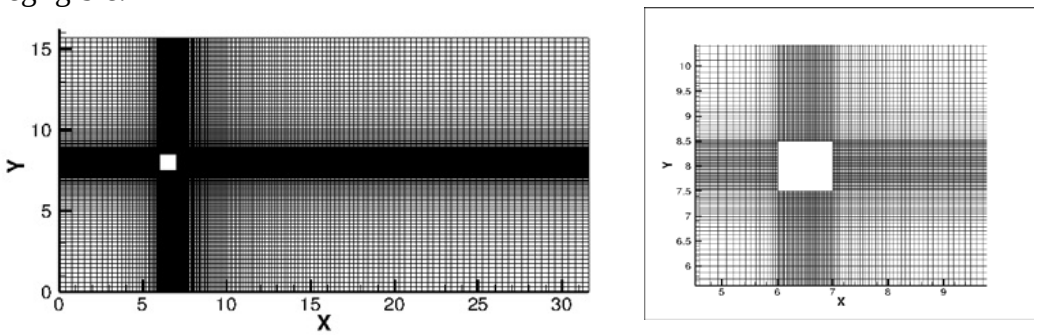

2a. 2b.

Figure: 2a. Non-uniform structured grid for discretization of the domain. 2b. Closer view of the grid point collocation at the wall of the step for accurate resolution of the boundary layer.

Figures 2(a), (b), present the grid of the proposed problem. Figure 2(a), clearly shows the four subdomains used to generate the grid. The first subdomain is the region upstream of the square cylinder which includes the horizontal splitter plate. The second and third subdomains are the regions located just below and above the square cylinder respectively. The region downstream of the square cylinder is the fourth sub domain. Non-uniform structured grid has been generated in the four sub-domains using the stretching transformation proposed by Roberts (1971), which refines the grid in the vicinity of the solid walls

2.2 Governing Equations.

Non-dimensional form of the governing equations was used to simulate the flow. To non dimensionalize the equations, the side of the square cylinder, A, was taken as the characteristic length, the free stream velocity under the splitter plate at the inlet, U, was considered as the characteristic velocity, characteristic pressure was ρU^2 and characteristic time was defined as characteristic length divided by the characteristic velocity, A/U. Reynolds number, Re was defined as $\mathrm{Re} = \frac{\rho U A}{\mu}$. Fluid density, ρ and viscosity, μ were considered to be constant. Flow was regarded as isothermal.

The non-dimensional conservative form of the momentum and continuity equations for laminar flow, in two dimensions, reads:

$$\frac{\partial u}{\partial t} + \frac{\partial uu}{\partial x} + \frac{\partial vu}{\partial y} = -\frac{\partial p}{\partial x} + \frac{1}{\mathrm{Re}}\left(\frac{\partial^2 u}{\partial x^2} + \frac{\partial^2 u}{\partial y^2}\right) \tag{1}$$

$$\frac{\partial v}{\partial t} + \frac{\partial uv}{\partial x} + \frac{\partial vv}{\partial y} = -\frac{\partial p}{\partial y} + \frac{1}{\mathrm{Re}}\left(\frac{\partial^2 v}{\partial x^2} + \frac{\partial^2 v}{\partial y^2}\right) \tag{2}$$

$$\frac{\partial u}{\partial x} + \frac{\partial v}{\partial y} = 0 \tag{3}$$

Where u and v are the non-dimensional velocity components in X and Y direction, p is the non-dimensional pressure, x and y are non-dimensional Eulerian coordinates in the X and Y directions respectively. The non-dimensional time is denoted by t. A finite volume approach was chosen for the simulation.

2.3 Numerical Strategy and Boundary Conditions.

A second-order Adams Bashforth-Crank Nicholson scheme for temporal discretization was applied to Navier Stokes equations in finite volume formulation to obtain equation (4). Equation (5) is the continuity equation applied over a control volume.

$$\frac{u_{i,P}^{n+1} - u_{i,P}^{n}}{\Delta t} \forall_P + \left(\frac{3}{2}\sum_f F_f^n u_{i,f}^n - \frac{1}{2}\sum_f F_f^{n-1} u_{i,f}^{n-1}\right) = -\sum_f p_f^n S_{f,i} + \frac{1}{2\,\mathrm{Re}}\left(\sum_f F_{dfi}^{n+1} + \sum_f F_{dfi}^{n}\right) \tag{4}$$

$$\sum_f F_f^{n+1} = 0 \tag{5}$$

Where F_f represents the flux through the face f. Subscript P represents the center of the control volume with volume, $\forall$.

The boundary conditions used in the simulation were depicted in figure 1; a brief description of the different boundary conditions follows.

At the inlet, free stream condition for velocity and Neumann boundary condition for pressure were used. Equation (6) was used below and equation (7) above the splitter plate.

$$u = u,\ v = 0,\ \frac{\partial p}{\partial x} = 0 \tag{6}$$

$$u = ru,\ v = 0,\ \frac{\partial p}{\partial x} = 0 \tag{7}$$

A no-slip boundary condition was applied on solid boundaries as presented in equation (8)

$$u = 0, v = 0 \text{ and } \nabla p.\hat{n} = 0 \tag{8}$$

Where $\hat{n}$ is the unit normal vector perpendicular to the surface.

In the far field, since in the present study flow past a square cylinder is unconfined, a frictionless wall boundary was considered at a distance 8a measured from the center of the square cylinder, as shown in figure 1

$$\frac{\partial u}{\partial y} = 0 \text{ , v=0 and } \frac{\partial p}{\partial y} = 0 \tag{9}$$

The outlet boundary is of paramount importance when studying flows with unsteady wake or convecting vortices, since it not only changes the flow pattern but also affects convergence. In the present case the Newman boundary condition (NBC) was used for all dependent variables, as presented in equation (10).

$$\frac{\partial \phi}{\partial x} = 0,\ \phi = u, v, p \tag{10}$$

A 200x150 grid was used for all the simulations carried out in the present study, with 50 cells on the square cylinder's sides in both the x and y directions. The time step considered was dt=0.001. In the present study the respective pressure correction factors in all the neighboring cells were considered, this is an improvement of the original MAC (Marker and Cell) method, presented by Harlow and Welch (1965), to minimize the error involved in the calculation.

Lift and drag coefficients evaluate the average normal and shear stresses acting on the sides of the square cylinder. To calculate lift and drag coefficients, the expressions presented in equation (11) were used. It is important to realize that as the flow under study is unsteady and periodic, hence the concept of average lift and drag coefficients has to be used.

$$C_D = \frac{F_D}{\frac{1}{2}\rho U^2 A^2},\ C_L = \frac{F_L}{\frac{1}{2}\rho U^2 A^2}; \tag{11}$$

F_D and F_L are respectively the dimensional drag and lift forces due to the pressure and shear stresses acting on the square cylinder. Drag force was taken as positive when acting in the positive X axis direction, and lift force was regarded as positive when acting in the positive

Y axis direction. The equation to derive Strouhal number, St is presented as equation (12), f being the vortex shedding frequency in the square cylinder wake.

$$St=\frac{f\ A}{U} \qquad (12)$$

3. Code Validation.

The code was validated by simulating the unconfined flow past a square cylinder, under upstream uniform free stream flow. The results were compared with the ones presented in the existing literature. It was observed that the flow was steady for Reynolds numbers 50 and 52, see figure 3, and unsteady periodical at Re=55. According to Sohankar et al (1998), Von Karman vortex street appeared and therefore vortex shedding was happening in the wake of the square cylinder at Re=51.2±1. Kelkar and Patankar (1992) via flow stability analysis, found that the critical Reynolds number for the onset of vortex shedding was 54, which is in line with the results obtained and presented in figure 3.

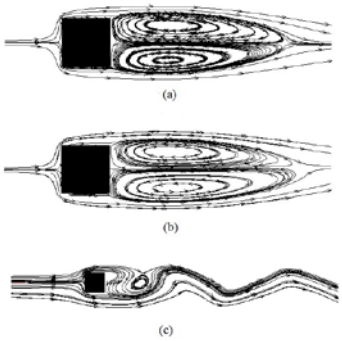

Figure: 3. Steady state streamlines plots of flow past a square cylinder, (a) Re=50, (b) Re=52, (c) unsteady periodic streamlines Re=55

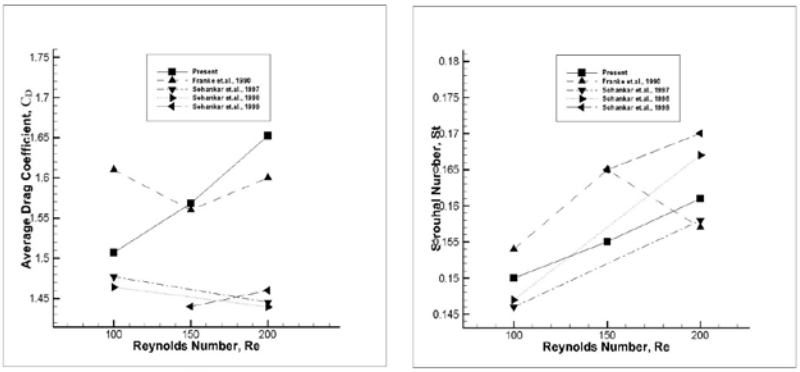

Figure: 4. (a) Average drag coefficient, C_D versus Reynolds number (b) Strouhal number, St plots versus Reynolds number for unconfined flow past a square cylinder.

For unconfined flow past a square cylinder in an unsteady periodic flow regime under the Reynolds number range 100≤Re≤200, average drag coefficients and Strouhal numbers were compared with the results presented by Franke et al (1990) and Sohankar et al (1997; 1998; 1999). In all cases identical flow and boundary conditions were used. Figures 4(a), (b) present the Drag coefficient, C_D and Strouhal number, St versus the upstream flow Reynolds number. The present work and the research undertaken in the four previous

papers are compared. The present results compare well with the published literature, especially in the case of Strouhal number, which can be considered as a stringent parameter for comparison.

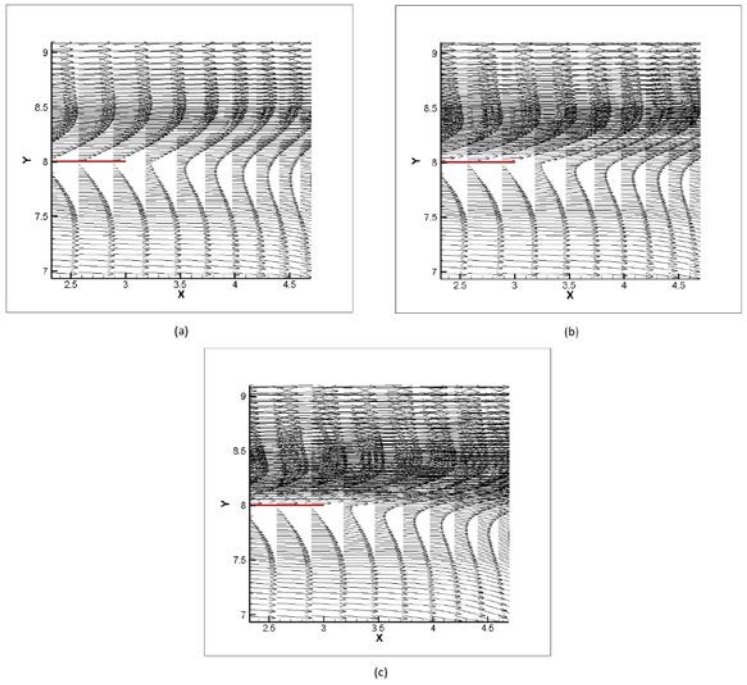

Figure: 5. Boundary layer and mixing layer development vector plots of flow over the splitter plate at Reynolds number, Re=100 for (a) r=2 (b) r=3 and (c) r=4.

The development of the laminar boundary layer and mixing layer behind the splitter plate can be seen in the vector plots presenting the flow over the splitter plate and upstream of the square cylinder for a Reynolds number, Re=100 and ratios, r=2, 3 and 4, figure 5. The development of Blasius profile of velocity gradient in the boundary layer over the splitter plate, as expected from a laminar boundary layer, can be clearly seen in figure 5 and validates the formation and development of the laminar boundary layer over the splitter plate. The fully developed boundary layers above and below the splitter, merge into a mixing layer in the wake of the splitter plate, due to the difference in the free stream velocities above and below splitter plate, which interacts with the flow in the wake of the square cylinder.

3.1 Effects of Grid Refinement:

A grid refinement study was carried out on three progressively refined grids for Re=200 and r=4, namely 180×120, 200×150 and 240×180, where the number of grid nodes distributed over the side of the square cylinder are 40, 50 and 60 respectively, cell widths are given in brackets.

Grid	180x120	200x150	240x180
No. of Cells on square side	40 (0.025)	50 (0.020)	60 (0.017)
Drag Coefficient	19.125	19.412	19.490

Table 1: Results of the grid refinement study

The variation in the drag coefficient, C_D was around 1.5% when the grid was refined from coarsest to the intermediate level. But when the grid was further refined to the finest level, the variation reduced further and became close to 0.4%, see table (1). Therefore, this has led to the use of a grid size of 200x150 for all the simulations.

4. Results and Discussion.

4.1 Unsteady periodic flow of wake and mixing layer interactions:

In order to evaluate unsteady periodic vortex shedding, simulations were carried out for Reynolds numbers 100, 150 and 200, for each Reynolds number velocity ratios of r = 1.5, 2, 2.5, 3, 3.5 and 4 were considered. For each case, three different upstream lengths of ul=5a, 6a and 7a, measured between the free stream inlet and the square cylinder leading edge, were studied. Additionally, velocity ratios of r=1.6, 1.8, 1.9, 2.6, 2.8, 2.9, 3.6, 3.8 and 3.9 were also evaluated for ul=6a and ul=7a. When studying flow past a square cylinder, Okajima et al (1992) realized that, for a Reynolds number of Re=1000, flow instabilities suffered a sudden increase when compared to the flow patterns appearing at lower Reynolds numbers. Scarano et al (2009) studied the flow around a square cylinder experimentally and observed that the transitional Reynolds number between laminar and turbulent flow happened to be at Re=1080, below which the flow remained laminar. On the other hand, Sau (2009), Luo et al (2003) and Salinas et al (2014) reported the appearance of three dimensional structures at much lower Reynolds numbers. The authors of the present paper are very much aware that, especially for the higher Reynolds numbers and velocity ratios presented in the present research, the flow must be seen as three dimensional. Nevertheless, considering this is the first time this flow is being simulated on a wide range of parameters and having in mind the richness of the flow structures appearing, the evaluation of the flow in 2D shall be seen as the first step in understanding the proposed configuration.

A typical laminar periodic vortex shedding is presented in Figure 6, in the form of instantaneous vorticity and streamlines contour plots corresponding to six equally spaced time instants within a shedding cycle of time period T. The Reynolds number was taken as 100, the velocity ratio being r=1.5. The distance between the splitter plate and the square cylinder was considered to be 3 units, being the upstream length, ul = 6 units. Two types of inviscid critical points, namely ‘center’ and ‘saddle’ can be observed. A critical point is a location where the slope of streamline becomes indefinite; the point of zero velocity is referred to as the ‘center’ while the point where two streamlines running in opposite directions touch each other, is referred to as a ‘saddle’ point. From figure 6 it is clearly seen that the saddle point of a shed vortex disappears before a new vortex is shed. Instantaneous vorticity contours, further reveals the formation and shedding of vortices from the rear edge of the square cylinder. The positive and negative vorticity, corresponding respectively to counter-clockwise and clockwise motion, are presented by solid and dashed lines. The two vortices in the rear of the cylinder exhibit a flapping motion while the mixing layer moves into these growing vortices in the wake, only to be convected downstream in the form of a vortical structure which scales with the height of the cylinder.

As seen in figure 6 for ratio r=1.5, the vortex shedding occurs alternatively with positive and negative moment vortices. It was also found that alternate shedding was occurring at ratios r=1.6 to 1.9, ul=6a. A similar shedding pattern was found for ul=5a and 7a for r<2.

As velocity ratio increased, the dissipation frequency of positive moment vortices decreased before finally being dissipated as Kelvin-Helmholtz (KH) instability. This was found to be occurring from ratio r=2 and above. Figure 7 presents the case when r=4, where the KH instability was more prominent. According to the results obtained, the threshold velocity ratio separating the cases for which positive and negative vortices are dissipated alternatively into the wake, and the cases in which only negative moment vortices are being shed and the positive moment vortices are being shed as Kelvin-Helmholtz instability, was found to be around r =2, such threshold remained constant for the three upstream lengths and Reynolds numbers studied, ul=5a, ul=6a, ul=7a, Re=100, 150 and 200.

When comparing the results obtained at different ratios, it was observed that whenever the ratio was below r=3, the vortex dissipation had a higher regularity, but the simulations at r >3, showed much faster and less organized vortex dissipation, as more random vortical structures were being dissipated in the wake. For these cases, the mixing layer formed upstream of the square cylinder, tended to break down before reaching the square cylinder, therefore inducing very random vortex shedding into the wake with no regular pattern or single shedding frequency, as presented in figure 11 from the FFT analysis of the drag signal. The same phenomenon appeared with the increase of Reynolds number, although the effect was much weaker than the similar one happening when the Reynolds number was maintained constant and the ratio r increased.

For ul=7a, Reynolds 100 and velocity ratio r=4, the mixing layer breaks just upstream of the square cylinder, creating random small vortical structures which are convected into the wake of the square cylinder and causing disorganized downstream vortex shedding. It was observed that the same phenomena occurred when ul=6a, ratio 4, but the Reynolds number was 150. This can be attributed to the fact that when ul=7a the mixing layer has a longer development length and therefore the shear stresses have more time to induce flow instabilities in the upstream mixing layer, causing it to break away. For ul=5a, the mixing layer was breaking upstream when r=4 and Reynolds number was 200. Therefore, it can be concluded that for shorter upstream lengths the mixing layer tends to break at higher Reynolds number. The breaking up of the mixing layer can be clearly seen with the help of the vorticity contours in figure 8 for ul=6a, Re=200.

So far, from the present study it has been observed that the free shear layers shed from top and bottom edges of the square cylinder become naturally unstable and roll up alternately to form a large scale Vortex Street. Detailed inspection of the wakes via flow visualization, show that there are a few distinct features in the flow structure for each of the studied cases. For the unmodified square cylinder, the separated shear layers are deflected inwards immediately after they pass the cylinder base. This is believed to be due to the lower fluid velocity and pressure behind the rear edge of the square cylinder. In this region, the roll up of the shear layer from the top side of the cylinder entrains fluid from the adjacent irrotational flow into the growing vortex. The resulting backflow, due to this fluid entrainment, engulfs the rear face causing the negative moment vortex to be shed downstream. A similar mechanism occurs for the shedding of the positive moment vortices. As a result of the present study, this phenomenon is observed to be occurring for ratios up to r=1.9. It can be noted that for these small velocity ratios, the upstream mixing layer is

too weak to alter the vortex formation mechanism already introduced above. In the next section this phenomenon will be addressed as the first oscillation mode.

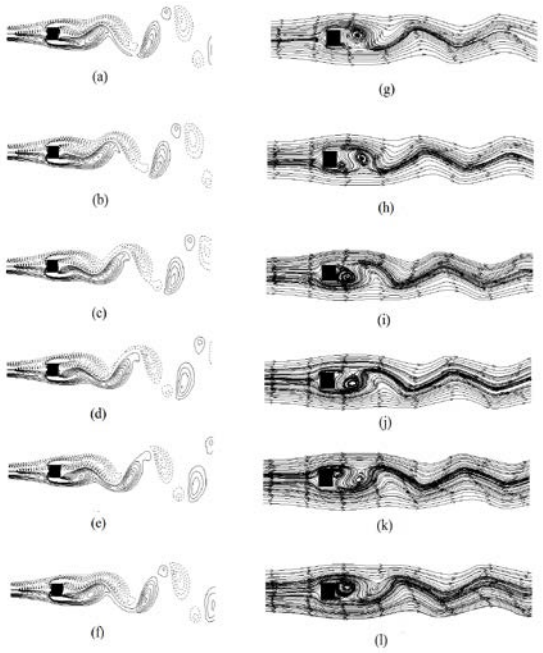

Figure (6): Vorticity and corresponding streamline plots of vortex shedding cycle in the wake of the square cylinder for ul=6a, Re=100 and r=1.5, (a, g) T/6; (b, h) T/3; (c, i) T/2; (d, j) 2T/3; (e, k) 5T/6; (f, l) T.

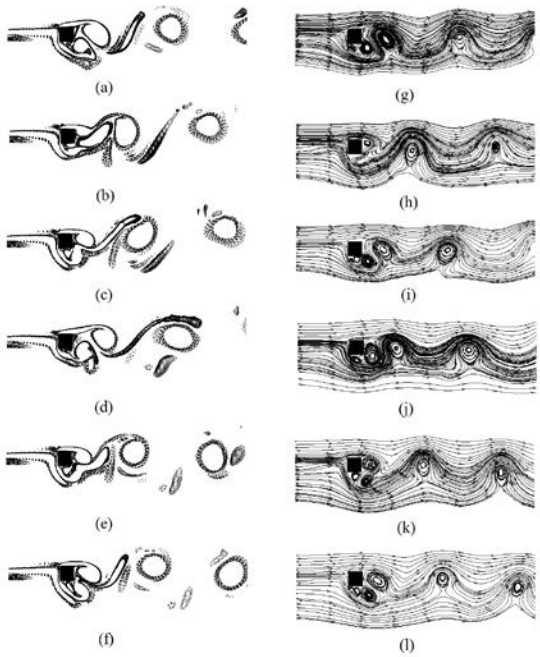

Figure (7): Vorticity and corresponding streamline plots of vortex shedding cycle in the wake of the square cylinder for ul=6a, Re=100 and r=4, (a, g) T/6; (b, h) T/3; (c, i) T/2; (d, j) 2T/3; (e, k) 5T/6; (f, l) T.

At higher ratios r, the interaction of the mixing layer with the laminar boundary layer emanating from the stagnation point, causes the free shear layer at the bottom of the square cylinder to separate at the lower corner of the front face, whereas the free shear layer on top of the square cylinder is attached to the surface and separates at the rear vertex of the top edge. This causes the positive vortex formed at the bottom of the square cylinder to become unstable, tending to break away from the free shear layer before reaching the rear edge of the square cylinder, as seen in figure 7. Since the energy associated with the primary vortex is much higher than that corresponding to the secondary vortex, the primary vortex grows faster and entrains into the slowly growing secondary vortex at the bottom of the square cylinder, causing it to be dissipated as Kelvin-Helmholtz instability. This phenomenon of vortex shedding was found to occur for a relatively stable mixing layer; the breaking of the mixing layer upstream was not observed. For Re=100 and ul=6a, the shedding mechanism explained above, was found to be occurring from r=2 until r=3.9. As ratio r increased, the stagnation point tended to move up on the front face of the square cylinder, causing the laminar boundary layer to separate before reaching the lower corner of the front face.

The flow structures around the front and side faces of the square cylinder are qualitatively unchanged when the splitter plate is moved upstream of the square cylinder. On the front

face, a well-defined stagnation point was observed in all cases. From this point, the fluid is forced to move over the body and laminar boundary layers are developed along the front surface. At the front corners of the square cylinder, the abrupt change in geometry induces separation and free shear layers are initiated at these points. From figures 6 to 8 a distinct stagnation point was observed for each case on the square cylinder front face. The stagnation point displacement as a function of the velocity ratio r, ul=6a and for a Reynolds number 100, is presented in figure 9. From figure 7, Re=100 and r=4, considering the streamlines plots 7g to 7l, minor variations with respect to the change in the stagnation point position can be observed. In one periodic shedding cycle, the stagnation point oscillates between the positions (6; 8.25) and (6; 8.38), measured from the coordinate axes' origin, see figure 2b. This stagnation point oscillation is attributed to the unstable oscillating upstream mixing layer, which tends to break. In figure 8, for Re=200 and ratio r=4, the stagnation point oscillates between the top and bottom corner of the square cylinder front face, positions (6; 8.1) and (6; 8.45). It can be noted that the stagnation point oscillation amplitude for this second case is about three times bigger than for the previous one. This is due to the breaking up of the mixing layer upstream of the square cylinder, which induces a wavering motion of the vortical structures generated upstream in tandem with the vortices generated on the rear edge of the square cylinder. At this ratio r=4, the free shear layer generated at the bottom of the square cylinder becomes unstable and separates before reaching the leading edge lower corner. As a consequence, the positive vortex at the bottom of the square cylinder separates before reaching the rear edge of the square cylinder as it interacts with the breaking mixing layer formed upstream, causing a very random and unstructured vortex dissipation in the wake of the square cylinder as seen in the vorticity plots in figures 7 and 8 when compared to figure 6. This random dissipation will be clearly seen from the FFT analysis of the drag coefficient presented in figure 11.

Due to the high velocity ratio, r=4, the negative vortical structures generated by the breaking mixing layer interact with the positive vortex produced by the free shear layer at the bottom of the square cylinder, suppressing its formation. As a result, the vortices generated at the bottom of the square cylinder are weakened while the vortices formed at the top are shed downstream as primary vortical structures. Despite the fact that the incoming negative vortical structures tend to weaken the positive vortex generated below the square cylinder, the positive vortical structures gradually grow in size until they are eventually shed downstream as KH instability.–During the vortex growing process, the stagnation point at the square cylinder front face moves downward. The lowest position of the stagnation point is reached when the vortex formed below the square cylinder is about to be shed. As soon as the vortex at the bottom is shed, the stagnation point moves up reaching its highest position and the cycle is repeated again.

Figure 9 summarizes the stagnation point oscillation as a function of the velocity ratio r for Re=100, ul=6a. Different oscillation patterns are associated to different amplitudes which depend on the velocity ratio r. The ranges of velocity ratios, r where the displacement amplitude of the stagnation point remains constant, will constitute an oscillation mode. The change in modes of dissipation is occurring at r = 1.9, 2.9, 3.9. Dissipation mode occurring from r = 1.5 to 1.9 will be called as mode 1, vortex shedding from r = 2 to 2.9 as mode 2, for 3< r <3.9 will be called mode 3 and at r = 4 is mode 4. A general trend characterizing all cases studied shows that as the ratio r increases from 1.5 to 4, the stagnation point's average

position tends to move upwards on the front face of the square cylinder. This phenomenon was previously reported by Cheng et al (2007), when studying plane shear flow around a square cylinder.

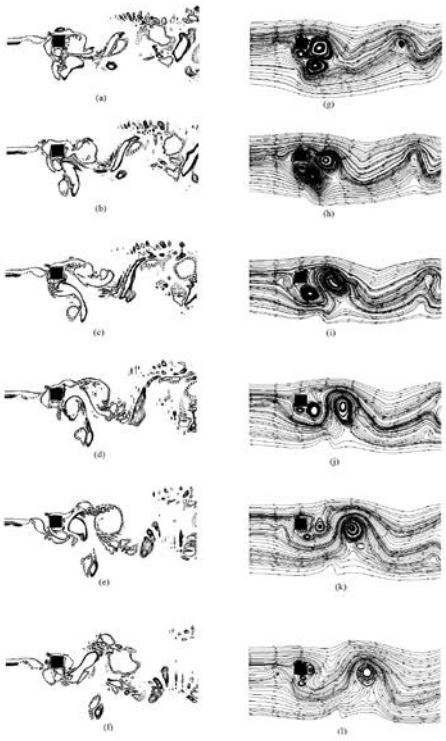

Figure (8): Vorticity contour and corresponding streamline plots of vortex shedding in the wake of the square cylinder for ul=6a, Re=200 and r=4, (a, g) T/6; (b, h) T/3; (c, i) T/2; (d, j) 2T/3; (e, k) 5T/6; (f, l) T.

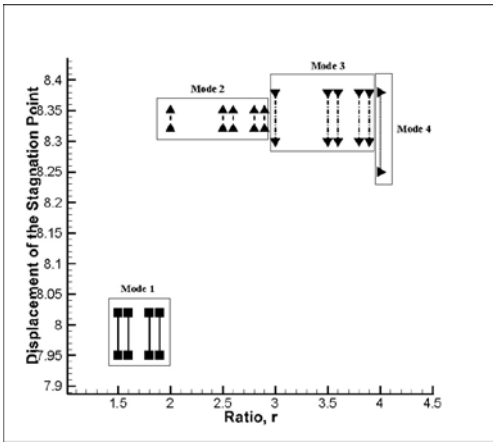

Figure (9): Displacement of the stagnation point vs. the Ratio, r for Reynolds number, Re=100 and upstream length, ul=6a

4.2 Lift and Drag Coefficients, C_D & C_L.

Figure 10 introduces the average lift, C_L and drag coefficients, C_D for all velocity ratios studied, ul=6a, Re=100, 150 and 200. The first observation to be made is that both coefficients exhibit a stepwise profile, indicating the existence of different modes of vortex dissipation in the wake of the square cylinder, as it was found in the case of the stagnation point oscillations.

At this point it is interesting to recall the work done by Williamson (1996), which presented that for an isolated circular cylinder placed in a laminar two dimensional flow, the transition from a two dimensional to a three dimensional laminar regime was characterized by two distinct discontinuities i.e. two different vibration modes. Sukri et al (2012) also found two oscillation modes when studying uniform flow around a square cylinder with a detached thin flat plate located downstream. Also, Malekzadeh and Sohankar (2012), when studying laminar flow around a square cylinder with a splitter plate located upstream, found three different oscillation modes. The existence of several oscillation modes in circular and

square cylinders have been found by many researchers but never for the conditions of the flow simulated and presented in the present paper.
Regarding the average drag coefficient, figure 10(a) shows that it increases with the increase of the ratio r, remaining constant for any given mode, regardless of the upstream value of Reynolds number. The occurrence of the different dissipation modes is to be attributed to the energy thresholds, sufficient to cause a different vortex shedding pattern in the wake. This phenomenon can also be observed from figure 9. The stagnation point's position oscillation has the same amplitude in a given mode until the energy associated to the flow increases and reaches a level which initiates the onset of a new mode. Similar variations in the upstream mixing layer behavior between different modes, can also be seen from the vorticity plots of Figures 6-8. In a given mode the stability of the upstream mixing layer remains constant and as the velocity ratio r increases, the upstream mixing layer becomes more unstable and finally tends to break before reaching the front face of the square cylinder at ratio r=4 as seen in figure 8.

The average lift coefficient presented in figure 10(b) follows the same main trend as the drag coefficient, for a given Reynolds number, as r increases, the average lift coefficient increases due to an increase in the pressure difference above and below the square cylinder. This can be attributed to the fact that as the ratio r increases, the velocity over the top surface of the square cylinder also increases, causing the normal pressure on the top surface to decrease with respect to the square cylinder bottom surface one, where the flow velocity remains quite constant. Consequently, the pressure difference between the top and bottom surfaces increases, leading to an increase of the body lift. Pressure differential between top and bottom remains rather constant for a given mode.

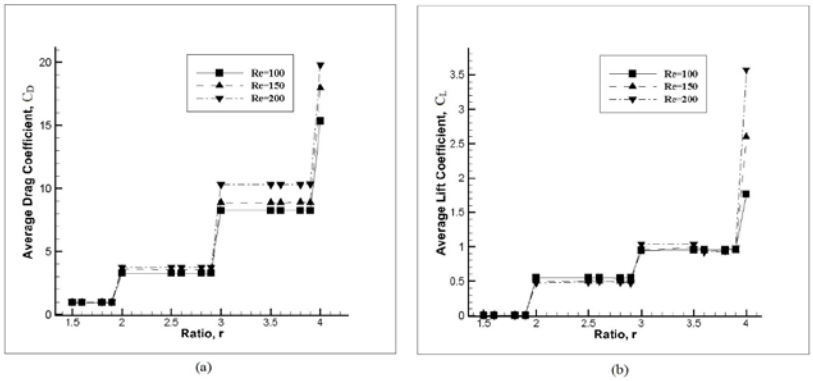

Figure 10 (a) Average drag coefficient, C_{Davg} versus ratio, r. (b) Average Lift coefficient, C_{Lavg} versus ratio, r. Upstream length ul = 6a.

It is interesting to observe that at ratio r=4, the increase in average lift and drag coefficients, when compared to the increase suffered at smaller ratios, is very much affected by the increase of Reynolds number, see figures 10(a) and (b). Notice that at ratio r=4, the velocity difference between the upper and lower square cylinder surfaces is at its highest, therefore the pressure difference between both surfaces suffers a drastic increase, this pressure increase directly influences the lift coefficient. Nevertheless the velocity increase between the upper and lower square cylinder faces, cannot explain why at smaller velocity ratios, the lift coefficient remains rather constant, in a given mode and for different Reynolds

numbers. The explanation in fact relies on vortex shedding. At lower ratios the mixing layer is relatively stable and coupled with the stable shear layers on top and bottom of the square cylinder, which leads to smaller pressure fluctuations. But at r=4, as the Reynolds number increases from 100 to 200, the mixing layer becomes more unstable and breaks, inducing instability in the shear layers and causing larger pressure fluctuations, the result is a higher increase on the body average lift.

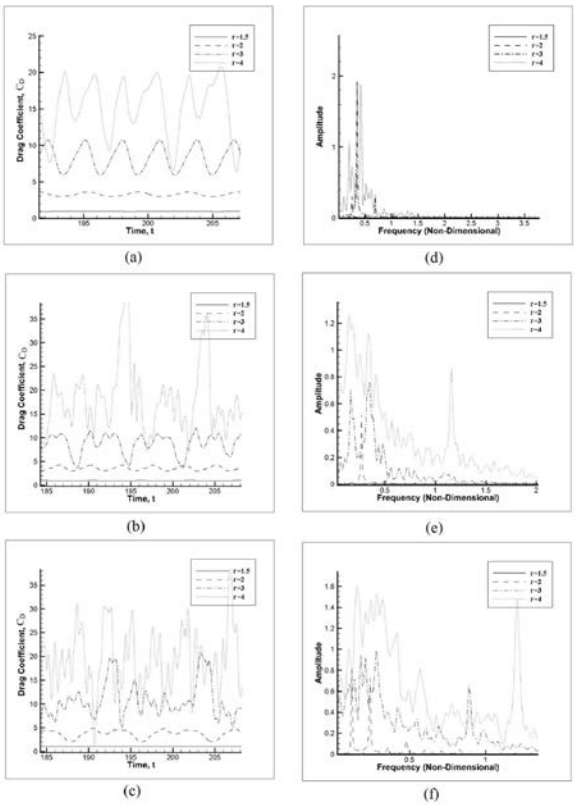

Figure 11: Drag coefficient versus time, as a function of upstream velocity ratio r. ul = 6a. (a) Re=100, (b) Re=150, (c) Re=200 and their respective FFT analysis in (d), (e) and (f)

Drag coefficient time dependent profiles, are introduced in figure 11 as a function of the velocity ratio r, and for the three upstream Reynolds numbers, ul=6a. It can be seen that the oscillation amplitude increases with the ratio r increase, the increase being over 80% when the ratio r is increased from 2 to 3. A very similar amplitude increase is spotted for the three Reynolds numbers studied Re=100, 150 and 200. For a given velocity ratio r, the oscillation amplitude also increases with the increase of the Reynolds number, although this increase is smaller than the one occurring when the velocity ratio r is modified. As an example, for r=2 and Reynolds number changing from 100 to 150, the oscillation amplitude increase is about 46%.

The increase of time dependent drag and lift oscillation amplitude as velocity ratio r increases is due of two main phenomena. The first one is an earlier shear layer separation from the square cylinder surfaces; the second one is the tendency of the mixing layer to break. These two factors complement each other causing higher pressure fluctuations, as can be seen from figures 11(d) to (f).

The Strouhal number, for all different velocity ratios and Reynolds numbers studied, is presented in figure 12 for upstream distances of ul=6a and 7a. For a given Reynolds, the Strouhal number increases with the increase of ratio r and remains constant for a given oscillation mode. This figure clarifies that each mode is characterized by a given vortex shedding frequency.

The evaluation of Strouhal number variation at a given mode, figure 12 (a), shows that in mode 1, for Re =100, the Strouhal number has a value of 0.15, and when Re =200, Strouhal number value is of 0.17. For velocity ratio, r =2, mode 2, when Reynolds number increases from 100 to 200, the Strouhal number increases about 38%. In mode 3, the Strouhal number increase when the Reynolds number goes from 100 to 200 is of 128% and at mode 4 the increase is about 103%.

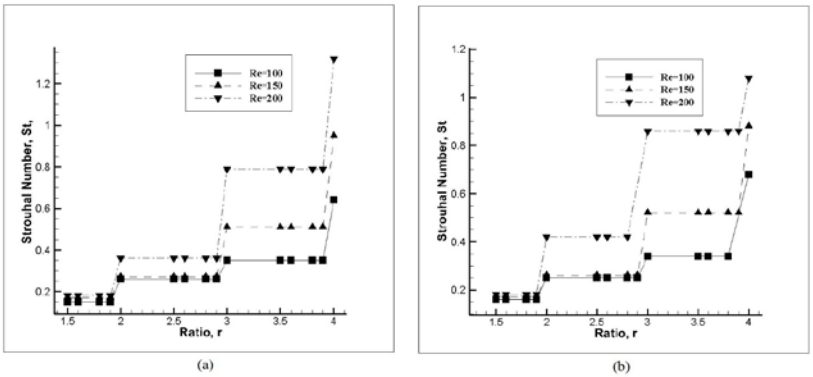

Figure 12: Strouhal Number, St versus Ratio, r for (a) ul=6a and (b) ul=7a

When comparing figures 12(a), (b), it can be seen that although the splitter plate distance increases, the modes of vibration still follow the same pattern, clearly indicating a global nature of the flow even in terms of Strouhal numbers. For a Reynolds number of 100, in mode 1, the increase of Strouhal number between ul=6a and ul=7a is of 6%, for mode 2 there is a small decrease of 3.8%, for mode 3 the decrease is 2.8% and for mode 4 there is an increase of 6%. Similar results are obtained for the other two Reynolds numbers studied. Since the Strouhal number variation with the increase of splitter plate distance is very small, it can be concluded that, for the cases studied, the splitter plate distance is not affecting the downstream vortex shedding frequency.

The increase in Strouhal number between two consecutive modes tends to increase for higher velocity ratios and higher Reynolds numbers, as an example, for a Reynolds number of 100, the Strouhal number increases about 80% when going from mode 1 to mode 2. This increase drops to 44% when moving from mode 2 to mode 3, and increases to 94% between modes 3 and 4. It was observed that in modes 1 and 2 the predominant effect when considering the Strouhal number change is due to the velocity ratio r, whereas in modes 3 and 4, the Reynolds number increase generates a higher variation in the Strouhal number. This is due to difference in the fluid kinetic energy above and below the splitter plate, which for ratios 3 and 4 is 8 and 15 times the kinetic energy below the splitter plate respectively. On the other hand, as the Reynolds number increases from 100 to 200, while maintaining the same two ratios, the value of kinetic energy increase between above and

below the splitter plate, is respectively 32 times and 60 times the kinetic energy below the splitter plate at Re=100.

Conclusions:

The wake and mixing layer interactions analyzed in the present study are primarily dependent on the velocity ratios. Four different modes of vortex dissipation were observed as the velocity ratio increased from 1.5 to 4. The vortex shedding mechanism in mode 1 was similar to the flow past a square cylinder with shedding of positive and negative moment vortices alternatively due to smaller velocity ratios. In the case of modes 2, 3 and 4, however, only negative vortices are shed downstream and the positive moment vortices are dissipated in the form of Kelvin-Helmholtz instabilities. The onset of Kelvin-Helmholtz instabilities in the wake occurs at velocity ratio 2, independent of the upstream Reynolds number and length, ul. Physical characteristics of the flow such as upstream mixing layer, stagnation point oscillation amplitude, vortex shedding pattern, Strouhal number and average lift and drag remain constant in any given mode. The tendency for the free shear layer to separate before reaching the lower vertex of leading edge, increases with the increase of ratio r. It was observed that the stagnation point moves upwards on the square cylinder's front face as the ratio r increases. A sudden variation in the position of the stagnation point was observed from mode 1 to mode 2, due to the change in the vortex shedding mechanism. Since the instability of the upstream mixing layer increases as the flow progresses from mode 2 to 4, the stagnation point oscillation amplitude also increases.

References:

Ayukawa, K., Ochi, J., Kawahara, G., Hirao, T. (1993). “Effects of shear rate on the flow around a square cylinder in uniform a shear flow,” J. Wind Engineering and industrial Aerodynamics. 50: 97-106.

Bhattacharyya, S., Maiti, D.K. (2004). “Shear flow past a square cylinder near a wall.” International Journal of Engineering Science 42, 2119-2134.

Bhattacharyya, S., Maiti, D.K. (2006). “Vortex shedding suppression for laminar flow past a square cylinder near a plane wall: a two-dimensional analysis,” Acta Mechanica 184: 15-31.

Cheng, M., Tan, S.H.N., Hung, C. (2005). “Linear shear flow over a square cylinder at low Reynolds number,” Physics of Fluids 17: 078103-1/4.

Cheng, M., Whyte, D.S., Lou, J. (2007). “Numerical simulation of flow around a square cylinder in uniform-shear flow,” Journal of Fluids and Structures. 23: 207-226.

Davis, R.W., Moore, E.F. (1982). “A numerical Study of vortex shedding from rectangles,” J Fluid Mech. 116; 475-506.

Davis, R.W., Moore, E.F., Purtell, L.P. (1984).“A numerical-experimental study of confined flow around rectangular cylinders,” Phys. Fluids. 27: 46-59.

Doolan, C.J. (2009). “Flat-plate interaction with the near wake of a square cylinder,” AIAA Journal. 47;2: 475-478.

Franke, R., Rodi, W., Schonung. B. (1990). “Numerical calculation of laminar vortex shedding flow past cylinders,” Journal of wind energy and industrial Aerodynamics. 35, 237-257.

Franke, R. (1991). “Numerische Berechnung der instationären Wirbelablösung hinter zylindrischen Körpern,” Ph.D. Thesis, University of Karlsruhe.

Harlow, F.H., Welch. J.E. (1965). “Numerical calculation of time-dependent viscous incompressible flow of fluid with free surface”. Physics of Fluids. 8, 2182-2189.
Hwang, R.R., Sue. Y.C. (1997). “Numerical simulation of shear effect on vortex shedding behind a square cylinder,” Int. J. for Numerical Methods in Fluids. 25:12, 1409-1420.
Jordan, S.K., Fromm, J.E. (1972). “Laminar flow past a circle in a shear-flow,” Physics of Fluids, 15:6, 972.
Kelkar, K.M., Patankar, S.V. (1992). “Numerical prediction of vortex shedding behind a square cylinder,” International Journal for Numerical Methods in Fluids, 14, 327-341.
Kiya, M.; Tamura, H., Arie, M. (1980). “Vortex shedding from a circular cylinder in moderate-Reynolds number shear flow,” J Fluid Mech, 141:4, 721-735.
Kwon, T.S.; Sung, H.J., Hyun, J.M. (1992). “Experimental investigation of uniform-shear flow past a circular cylinder,” J Fluids. Eng, 114, 457.
Lankadasu, A., Vengadesan, S. (2008). “Onset of vortex shedding in planar shear flow past a square cylinder,” Int. Journal of Heat and Fluid Flow, 29, 1054-1059.
Lesage, F.; Gartshore, I.S. (1987). “A method of reducing drag and fluctuating side force on bluff bodies,” Journal of Wind Engineering and Industrial aerodynamics, 25, 229-245.
Luo, S.C., Chew, Y.T., Ng, Y.T. (2003). “Characteristics of square cylinder wake transition flows” Physics of Fluids, 15, 2549.
Luo, S.C., Tong, X.H., Khoo, B.C. (2007). “Transition phenomena in the wake of a square cylinder,” J. of Fluids and Structures, 23, 227-248.
Malekzadeh, S., Sohankar, A. (2012). “Reduction of Fluid forces and heat transfer on a square cylinder in a laminar flow regime using a control plate,” Int. Journal of Heat and Fluid flow, 34, 15-27.
Mukhopadhyay, A., Biswa, G., Sundararajan, T. (1992). “Numerical Investigation of confined wakes behind a square cylinder in a channel,” International Journal for Numerical Methods in Fluids, 14, 1473-1484.
Mukhopadhyay, A., Venugopal, P., Vanka, S.P. (1999). “Numerical study of vortex shedding from a circular cylinder in linear shear flow,” J Fluid Engineering, 121:2, 462-468.
Okajima, A. (1982). “Strouhal numbers of rectangular cylinders,” J Fluid Mech, 123, 379-398.
Okajima, A. (1990). “Numerical simulation of flow around rectangular cylinders,” J. Wind Eng. Ind. Aerodyn, 33, 171-180.
Okajima, A., Ueno, H., Sakai, H. (1992). “Numerical Simulation of Laminar and Turbulent Flows around Rectangular Cylinders,” Int. Journal for Numerical Methods in Fluids, 15, 999-1012.
Roberts, G.O. (1971). “Computational meshes for boundary layer problems,” Proceedings of the second international conference on numerical methods and fluid dynamics, Lecture notes in physics, 8, 171-177, Springer-Verlag New York.
Saha, A.K., Biswas, G., Muralidhar, K. (2001). “Two dimensional study of the turbulent wake behind a square cylinder subject to uniform shear,” ASME J. Fluids Eng. 123:3, 595-603.
Sakamoto, H., Tan, K., Haniu, H. (1991). “An optimum suppression of fluid forces by controlling a shear layer separated from a square prism,” ASME J. Fluids Eng., 113:2, 183-189.
Sakamoto, H., Tan, K., Takeuchi, N., Haniu, H. (1997). “Suppression of fluid forces acting on a square prism by passive control,” ASME Journal of Fluids Engineering, 119, 506-511.

Salinas-Vazquez, M., Vicente, W., Barrera, E, Martinez, E. (2014). “Numerical Analysis of the drag force of the flow in a square cylinder with a flat plate in front”. Revista Mexicana de Física, 60, 102-108.
Sau A. (2009).“Hopf bifurcations in the wake of a square cylinder”, Physics of Fluids, 21, 034105.
Scarano, F., Poel, M.C. (2009). “Three-dimensional vorticity pattern of cylinder wakes,” Exp. Fluids, 47, 69-83.
Sohankar, A., Davidson, L., Norberg, C. (1995). “Numerical simulation of unsteady flow around a square two dimensional cylinder,” 12th Australian Fluid Mechanics Conference, University of Sydney, Australia, 517-520.
Sohankar, A., Norberg, C., Davidson. L. (1997). “Numerical Simulation of Unsteady low-Reynolds number flow around Rectangular cylinders at incidence,” Journal of Wind Engineering and Industrial Aerodynamics, 69:71, 189-201.
Sohankar, A., Norberg, C., Davidson, L. (1998). "Low Reynolds number flow around a square cylinder at incidence: Study of blockage, onset of vortex shedding and outlet boundary condition,” Int Journal for Numerical Methods in Fluids, 26, 39-56.
Sohankar, A., Norberg, C., Davidson, L. (1999). “Simulation of three-dimensional flow around a square cylinder at moderate Reynolds numbers,” Phys. Fluids, 11, 288-306.
Sukri, M.A.M., Doolan, C.J., Wheatley,V. (2011). “Low Reynolds number flow over a square cylinder with a splitter plate,” Phys. Fluids, 23, 033602.
Sukri, M. A. M., Doolan, C.J., Wheatley, V. (2012). “Low Reynolds number flow over a square cylinder with a detached flat plate,” International Journal of Heat and Fluid Flow, 36, 133-141.
Sumner, D., Akosile, O.O. (2003). “On uniform planar shear flow around a circular cylinder at subcritical Reynolds number,” J. Fluids and Structures, 18, 441-454.
Suzuki, H., Inoue, Y., Nishimura, T., Fukutani, K., Suzuki, K. (1993). “Unsteady flow in a channel obstructed by a square rod. (crisscross motion of vortex),” Int. Journal of Heat and Fluid Flow, 14:1, 2-9.
Williamson, C.H.K., “Vortex Dynamics in the Cylinder Wake,” Annu. Rev. Fluid Mech, 28, 477-539, (1996).
Xu, Y., Dalton, C. (2001). “Computational force on a cylinder in a shear flow,” Journal of Fluids and Structures, 15, 941-954.
Yoshida, T., Watanabe, T., Nakamura, I. (1993). “Numerical Analysis of open boundary conditions for incompressible viscous flow past a square cylinder,” Transactions of JSME, 59, 2799-2806.
Zhou, L., Cheng, M., Hung, K.C. (2005). “Suppression of fluid force on a square cylinder by flow control,” Journal of Fluids and Structures, 21, 151-167.